Available online at www.sciencedirect.com
ScienceDirect
Journal of Nuclear Materials 358 (2006) 176–189
journal of nuclear materials
www.elsevier.com/locate/jnucmat

Investigation of neutron radiation effects on the mechanical behavior of recrystallized zirconium alloys

F. Onimus [a,*], J.L. Béchade [a], C. Duguay [b], D. Gilbon [b], P. Pilvin [c]

[a] Service de Recherches Métallurgiques Appliquées, CEA-Saclay, 91191 Gif-sur-Yvette, France
[b] Service d'Etudes des Matériaux Irradiés, CEA-Saclay, 91191 Gif-sur-Yvette, France
[c] Laboratoire de Génie Mécanique et Matériaux, Université de Bretagne-Sud, 56321 Lorient, France

Received 20 March 2006; accepted 12 July 2006

Abstract

Neutron radiation induces important changes in the mechanical behavior of recrystallized zirconium alloys used as fuel cladding tube. The neutron radiation effects on the mechanical behavior for internal pressure tests performed at 350 °C have been investigated using a specific analysis in terms of isotropic hardening, kinematic hardening and viscous stress. A unified internal variables modeling has also been used in order to provide a consistent description of the radiation effects on the mechanical behavior. The impact of irradiation has been interpreted in terms of microscopic deformation mechanisms observed by transmission electron microscopy. Due to the localization of the plastic deformation inside channels and because of the only activation of basal channeling, the kinematic hardening is expected to be strong in irradiated zirconium alloys.

PACS: 61.80.Hg; 62.20.Fe

1. Introduction

Zirconium alloys cladding tubes containing the fuel of pressurized water reactors nuclear power plants constitute the first barrier against the dissemination of radioactive elements. In order to improve the material and guaranty the cladding integrity all along its life time, it is necessary to have a good understanding of the effect of neutron radiation on the mechanical properties and the related radiation-induced microstructure.

It is known that neutron radiation leads to a significant increase in strength [1–4]. This strengthening is usually attributed to the presence of a high density of small ⟨a⟩ prismatic loops induced by irradiation [5] which act as obstacles against dislocations glide [6,7]. However it is known that these loops can be swept up by gliding dislocations when a sufficient stress is applied leading to the creation of channels where dislocations can freely glide [8]. This mechanism has been reported by several authors in

* Corresponding author. Tel.: +33 1 69 08 44 29; fax: +33 1 69 08 71 30.
E-mail address: fabien.onimus@cea.fr (F. Onimus).

0022-3115/$ - see front matter © 2006 Elsevier B.V. All rights reserved.
doi:10.1016/j.jnucmat.2006.07.005

irradiated Zr alloys [9–15]. Lately an extensive study [16,17] of this phenomenon has been performed on irradiated Zr alloys tested at 350 °C using transmission electron microscopy (TEM). It has been established that for the irradiated material strained during a tensile test performed in the transverse direction of a rolled sheet specimen or an internal pressure test performed on a cladding specimen at 350 °C, only basal channeling occurs whereas for the non-irradiated material, prismatic glide is mainly activated. The change in principal slip system activation has been attributed to the difference in junction reaction between loops and prismatic gliding dislocation and basal gliding dislocation. Indeed, as described in [16], in the hexagonal closed packed structure, the junctions created between a ⟨a⟩ loop and a ⟨a⟩ dislocation gliding in the basal plane are always glissile whereas in the case of a ⟨a⟩ dislocation gliding on the prismatic plane and interacting with a ⟨a⟩ loop, the junction is sessile in two cases over three. This leads to a lower ability for dislocation channeling in prismatic plane and therefore a change in principal slip system activation.

Nevertheless, the effect of this specific deformation mechanism on the mechanical behavior of irradiated zirconium alloys (for internal pressure test at 350 °C) is not yet clear.

In order to have a thorough understanding of the effect of dislocation channeling phenomenon on the mechanical behavior of neutron irradiated zirconium alloys, a detailed mechanical analysis has been performed. This specific analysis aims at characterizing the strain hardening behavior, the strain rate sensitivity as well as the stress relaxation behavior of the irradiated material and the non-irradiated material. A unified internal variables model is also used in order to confirm the analysis and provide a coherent description of the effect of neutron radiation on mechanical properties. The obtained results are then compared and discussed in terms of deformation mechanisms observed by TEM.

2. Materials and mechanical tests

Mechanical tests have been performed on three irradiated and non-irradiated recrystallized zirconium alloys: recrystallized Zy-4, M5^{TM} alloy and a previous experimental grade alloy referred here as Zr–1%Nb–O. Chemical compositions are given in Table 1 and irradiation conditions are given in Table 2.

Mechanical tests have been conducted at 350 °C at various strain rates with internal pressure loading condition ($\sigma_{zz} \approx \sigma_{\theta\theta}/2$ and $\sigma_{rr} \approx 0$). In addition, in order to obtain detailed information on the mechanical behavior, several non-monotonic tests have been performed. All these mechanical tests can be divided into four types. The first type of test is a simple monotonic strain hardening test (at a given

Table 1
Zr alloys chemical composition (wt%)

Alloy	Sn	Nb	Fe	Cr	O	Zr
Zy-4	1.30	–	0.210	0.100	0.125	Bal.
M5^{TM}	–	1.00	0.035	–	0.130	Bal.
Zr–1%Nb–O	–	1.00	0.02	–	0.125	Bal.

Table 2
Irradiation conditions and testing conditions

Specimen	Material	Fluence, n/m^2	Irradiation temperature (°C)	Mechanical test	Test temperature (°C)	Strain rate, s^{-1}
NI1	M5^{TM}	0	–	Type 4 at $\varepsilon = 0.8\%$	350	2.5×10^{-4}
NI2	M5^{TM}	0	–	Type 4 at $\varepsilon = 0.8\%$	350	2.5×10^{-4}
NI3	M5^{TM}	0	–	Type 4 at $\varepsilon = 0.8\%$	350	2.5×10^{-4}
NI4	M5^{TM}	0	–	Type 2 at $\varepsilon = 1.5\%$	350	2.0×10^{-4}
NI5	M5^{TM}	0	–	Type 2 at $\varepsilon = 2.3\%$	350	2.0×10^{-4}
NI6	M5^{TM}	0	–	Type 1	350	2.0×10^{-5}
NI7	M5^{TM}	0	–	Type 1	350	2.5×10^{-6}
NI8	Zy-4	0	–	Type 2 at $\varepsilon = 1.2\%$	350	2.5×10^{-4}
IR1*	M5^{TM}	3.5×10^{25}	350	Type 4 at $\varepsilon = 0.8\%$	350	3.0×10^{-4}
IR2	M5^{TM}	2.3×10^{25}	350	Type 4 at $\varepsilon = 0.8\%$	350	3.0×10^{-6}
IR3*	M5^{TM}	3.5×10^{25}	350	Type 3 at $\varepsilon = 0.8\%$	350	3.0×10^{-6}
IR4*	Zr–1%Nb–O	12×10^{25}	350	Type 1	350	3.0×10^{-4}
IR5*	Zy-4	0.4×10^{25}	350	Type 2 at $\varepsilon = 0.7\%$	350	3.0×10^{-4}

* TEM investigations [16,17]: basal channels observed.

strain rate) that can be followed (type 2) by an unloading stage beginning at a given strain ($\varepsilon_{\theta\theta}$) (with the same strain rate). The third type of test is a strain hardening test followed by a stress relaxation test at fixed strain ($\varepsilon_{\theta\theta}$) during 72 h. The relaxation test can also be followed (type 4) by another strain hardening test. Testing conditions are given in Table 2.

The stress and the strain are computed for internal pressure test using the usual thin wall formula. All stress and strain values given in the mechanical behavior analysis account for hoop stress ($\sigma_{\theta\theta}$) and hoop strain ($\varepsilon_{\theta\theta}$) of the biaxial stress state during internal pressure test.

On four out of the five irradiated specimens (IR1, IR3, IR4 and IR5), thin foils have been taken after testing and investigated using TEM. In each case many basal channels have been observed and no other type of channel can be observed. A detailed analysis is given in [16,17].

3. Mechanical behavior analysis

3.1. Yield and flow stress

Typical stress–strain curves of irradiated specimens are reported in Fig. 1, and compared to non-irradiated materials. Yield stress (chosen here at 0.02% plastic strain, $\sigma_{0.02\%}$) and flow stress at 0.2% plastic strain ($\sigma_{0.2\%}$) have been measured and are given in Table 3. Errors on the measurement

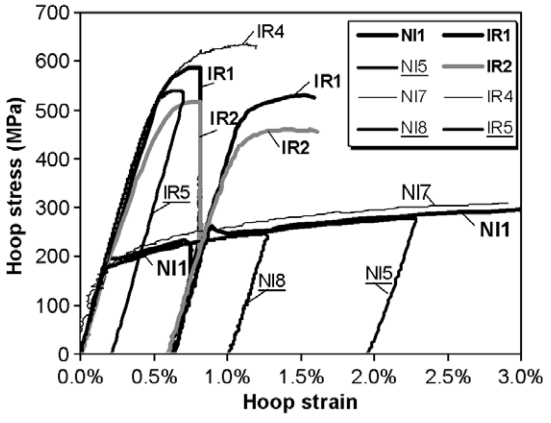

Fig. 1. Typical stress–strain curves (NI1, NI5, NI7, NI8, IR1, IR2, IR4, IR5) performed on non-irradiated and irradiated recrystallized Zy-4, M5^{TM} and Zr–1%Nb–O alloy. (Type 1: thin line, type 2: normal line, type 4: bold line). (The test IR4 performed on Zr–1%Nb–O alloy has been irradiated up to higher fluence.)

Table 3
Yield stress ($\sigma_{0.02\%}$) and flow stress ($\sigma_{0.2\%}$) of the eight non-irradiated specimens and the five irradiated specimens

Specimen	$\sigma_{0.02\%}$, MPa	$\sigma_{0.2\%}$, MPa
NI1	195 ± 5	205
NI2	190 ± 5	215
NI3	195 ± 5	215
NI4	200 ± 5	205
NI5	175 ± 5	200
NI6	180 ± 5	210
NI7	180 ± 5	210
NI8	175 ± 5	200
IR1	460 ± 20	590
IR2	320 ± 20	505
IR3	380 ± 20	510
IR4	460 ± 20	575
IR5	430 ± 20	540

of the yield stress given in Table 3 are due to uncertainty in determining the elastic slope for each test. The uncertainty is higher for the irradiated material due to the higher strain hardening rate at the onset of plastic flow.

As reported by many authors [1–4], it is shown that irradiation leads to a strong increase in flow stress, while elastic properties remain unaffected by irradiation. It is also seen that, the flow stress at 0.2% plastic strain increases as the irradiation fluence increases from 0.4×10^{25} to 12×10^{25} n/m^2. It can also be noticed that for the non-irradiated material, the difference between yield stress ($\sigma_{0.02\%}$) and flow stress ($\sigma_{0.2\%}$) is low (between 5 and 30 MPa), whereas after irradiation the difference between these two stresses becomes higher (between 110 and 185 MPa). This shows that the strain hardening is higher for the irradiated material than for the non-irradiated material between 0.02% and 0.2% plastic strain.

3.2. Strain hardening

In order to investigate the strain hardening behavior more accurately, the strain hardening rate has been computed and compared to the non-irradiated material. The strain hardening rates ($d\sigma/d\varepsilon^p$), for the two tests NI2 and IR1, are plotted as a function of the stress as reported in Fig. 2. It is shown that the strain hardening rate is nearly two orders of magnitude higher for the irradiated material ($d\sigma/d\varepsilon^p \approx 800$ GPa) than for the non-irradiated material ($d\sigma/d\varepsilon^p \approx 10$ GPa) at the onset of plastic flow. For the irradiated material however the strain hardening rate decreases rapidly to low values

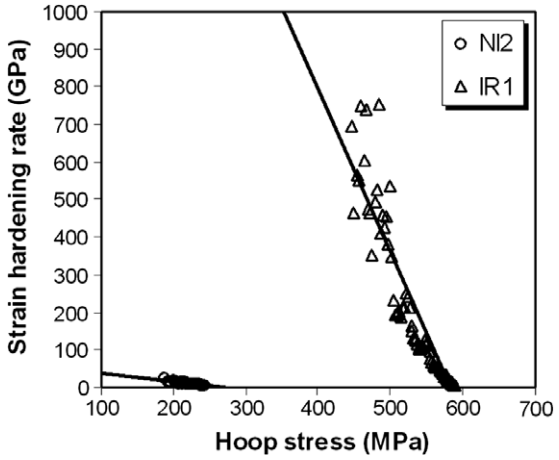

Fig. 2. Strain hardening rate vs. hoop stress for the two tests NI2 and IR1.

($d\sigma/d\varepsilon^p \approx 10$ GPa), whereas for the non-irradiated material, the strain hardening rate decreases slowly. As shown in Fig. 2, the decrease of the strain hardening rate follows a nearly linear relationship. The slope and the ordinate at origin, given in Eq. (1), are reported in Table 4.

$$\frac{d\sigma}{d\varepsilon^p} = -A\sigma + B. \quad (1)$$

Since the raw experimental signal exhibits strong fluctuations, a direct fitting approach may be preferred to the computation of the derivative of the stress with respect to the plastic strain. The integrated form of the differential equation (1) leads to Eq. (2), which is expressed here in terms of three parameters C, D and σ_0. These parameters are chosen so as to be compared to the coefficients obtained using a simple internal variables modeling described in the next section of this paper. For consistency, Eq. (1) can be rewritten in terms of these three coefficients in Eq. (3).

$$\sigma(\varepsilon^p) = \sigma_0 + \frac{C}{D}(1 - \exp(-D\varepsilon^p)), \quad (2)$$

$$\frac{d\sigma}{d\varepsilon^p} = -D\sigma + (D\sigma_0 + C). \quad (3)$$

Both methods give similar results (Table 4). It is shown that coefficients D and C are much higher for the irradiated material than for the non-irradiated material due to the higher strain hardening rate at the onset of plastic flow for the irradiated material. In the case of the specimen IR4, the data are not good enough to compute the strain hardening rate.

The results are in agreement with the data given by Yasuda et al. [3] who observed that irradiated recrystallized Zy-2 tested in axial tensile test exhibits a higher strain hardening coefficient at the onset of plastic flow than the non-irradiated material. It is also shown in [3] that the strain hardening coefficient decreases when the plastic strain increases, becoming lower (at the same plastic strain) than the strain hardening coefficient of the non-irradiated material.

3.3. Isotropic and kinematic hardening

It is known that during cyclic mechanical test, such as tensile-compressive test, many materials exhibit a Bauschinger effect leading to a lower yield

Table 4
Parameters obtained by the strain hardening rate analysis

Test	First method		Second method			
	$B = D\sigma_0 + C$ (MPa)	$A = D$	σ_0 (MPa)	C (MPa)	D	$B = D\sigma_0 + C$ (computed) (MPa)
NI1	3.2×10^4	105	180	1.43×10^4	130	3.8×10^4
NI2	5.4×10^4	195	185	1.56×10^4	130	4.0×10^4
NI3	6.2×10^4	230	190	1.35×10^4	120	3.6×10^4
NI4	4.0×10^4	140	190	1.34×10^4	130	3.8×10^4
NI5	3.3×10^4	115	175	1.29×10^4	115	3.3×10^4
NI6	4.4×10^4	145	180	1.69×10^4	125	3.9×10^4
NI7	3.4×10^4	105	180	1.56×10^4	125	3.8×10^4
NI8	1.8×10^4	160	175	1.30×10^4	130	3.6×10^4
IR1	1.2×10^6	4340	230	15.5×10^5	4300	2.5×10^6
IR2	1.1×10^6	2200	230	6.0×10^5	2000	1.1×10^6
IR3	2.0×10^6	3270	260	7.5×10^5	3000	1.5×10^6
IR4	–	–	230	15.5×10^5	4300	2.5×10^6
IR5	1.0×10^6	3920	230	13×10^5	4200	2.3×10^6

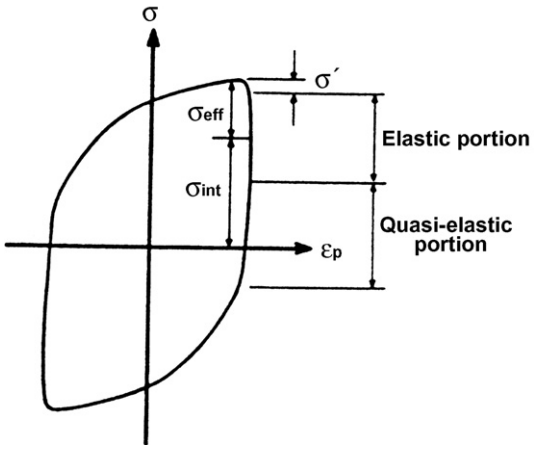

Fig. 3. Handfield and Dickson technique for interpreting hysteresis loop shape (from Handfield et al. [21]).

stress in compression performed after a tension than without prior tension. This phenomenon can be described, as proposed by [18–22] on the assumption that the flow stress is the sum of two components: the isotropic stress (R or effective athermal stress) and the kinematic stress (X or internal stress or back stress) referred as σ_{int} in Fig. 3

$$\sigma = X + R. \tag{4}$$

In addition to these two components, Dickson et al. [21] have proposed to add a third component (Fig. 3) which corresponds to the viscous stress (σ_V or the thermally activated stress [22]) referred as σ' in Fig. 3

$$\sigma = X + R + \sigma_V. \tag{5}$$

This component of the flow stress is revealed at the beginning of the unloading as a non-linear or quasi-elastic phase before the proper elastic phase.

In the case of non-irradiated Zr alloys, several authors have reported a strong Bauschinger effect [23–25]. For internal pressure test it is not possible to achieve proper reverse loading, such as compression test. Nevertheless, the reverse yield stress can be observed during the unloading if the kinematic stress (X) is higher than the isotropic stress (R). In that case it is possible to measure the kinematic stress as the value of the stress at the middle of the linear part of the unloading, the isotropic stress corresponding to half of the linear part of the unloading (Fig. 3).

On tests performed with unloading (type 2 tests), viscous (σ_V), isotropic (R) and kinematic (X) stresses have been measured (Table 5) as shown in Figs. 4–6. It has to be emphasized that this method leads to high uncertainty on the obtained values due to difficulties in determining the linear part of the unloading.

Table 5
Estimates for isotropic, viscous and kinematic stresses

Test	ε^p (%)	σ_V (MPa)	R (MPa)	X (MPa)	σ (MPa)
NI8	1	20 ± 20	70 ± 20	155 ± 20	245
NI4	1.2	20 ± 20	70 ± 20	175 ± 20	265
NI5	2	20 ± 20	70 ± 20	185 ± 20	275
IR5	0.2	70 ± 20	$R \geqslant 235$	$X \leqslant 235$	540

It is shown that for the non-irradiated material (assuming that recrystallized Zy-4 and M5^{TM} behave in the same manner) the viscous and isotropic stress are nearly constant with plastic strain, whereas the kinematic stress increases with plastic strain since it is assumed that the kinematic stress is equal to zero for zero plastic strain. The measured data are in agreement with the results obtained in

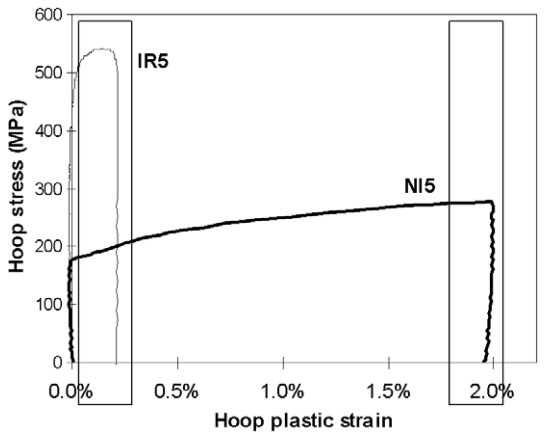

Fig. 4. Stress–plastic strain curves of the two loading–unloading tests NI5 and IR5.

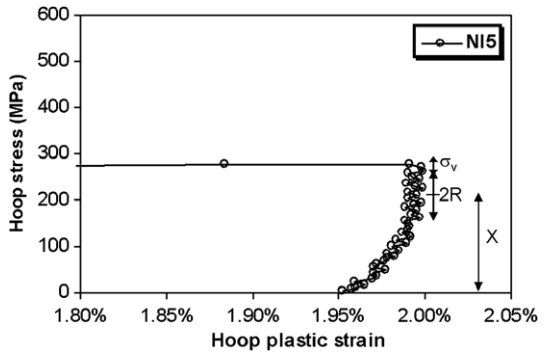

Fig. 5. End of the stress–plastic strain curve of the NI5 test.

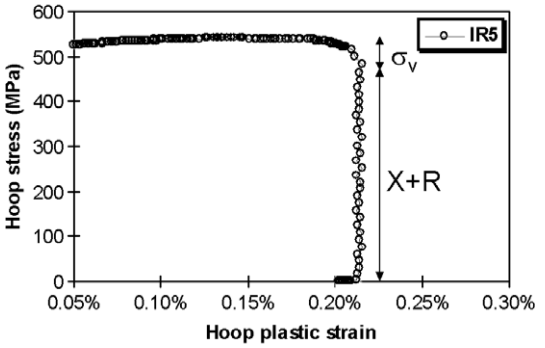

Fig. 6. End of the stress–plastic strain curve of the IR5 test.

[23–25] in low cycle fatigue at room temperature on various zirconium alloys. Indeed, it is shown in [23–25] that the back stress (X) is high in Zr alloys and the strain hardening is mainly due to the increase of the back stress, whereas the isotropic hardening is low.

The unloading test performed on the irradiated material (IR5) did not exhibit any sign of Bauschinger effect, as shown in Fig. 6. This proves that for this plastic strain level the kinematic stress is lower than the isotropic stress ($X \leqslant R$). The measured value of the flow stress ($\sigma_{0.2\%} = 540$ MPa) allows to evaluate the maximum value for the kinematic stress and the minimum value for the isotropic stress, taking into account that the measured viscous stress is of the order of $\sigma_V = 70 \pm 20$ MPa. It is then deduced that the isotropic stress is higher than 235 MPa and the kinematic stress is lower than 235 MPa for the irradiated material at 0.2% plastic strain.

3.4. Strain rate sensitivity

Mechanical tests performed at two different strain rates on non-irradiated and irradiated materials allow to compute the strain rate sensitivity of the materials. The strain rate sensitivity ($1/N$) can be expressed as

$$\frac{1}{N} = \frac{\Delta \ln(\sigma)}{\Delta \ln(\dot{\varepsilon}^P)}. \tag{6}$$

For the non-irradiated material, from values of the flow stress at 0.2% plastic strain for various strain rates (Table 3), it is shown that the strain rate sensitivity ranges from −0.013 to 0.005. These results agree with the data given in [24,26–31], where a very low strain rate sensitivity around 350 °C is observed. From data given in Table 3, it is shown that the strain rate sensitivity for the irradiated material ranges from 0.032 to 0.034.

Table 6
Strain rate sensitivity and Norton coefficient

Test	$1/N$	N
NI7, NI5, NI2, NI3	$-0.013 \leqslant 1/N \leqslant 0.005$	$N > 200$
IR1, IR2, IR3	$0.032 \leqslant 1/N \leqslant 0.034$	$31.6 \geqslant N \geqslant 29.6$

Assuming a Norton flow law (Eq. (7)), the Norton coefficient (N) can be computed as the inverse of the strain rate sensitivity. The Norton coefficient is therefore higher than 200 for the non-irradiated material and ranges from 29.6 to 31.6 for the irradiated material (Table 6). This increase of the strain rate sensitivity with irradiation has also been reported by Pettersson [32] for internal pressure tests performed at 290 °C

$$\dot{\varepsilon}^P = \left(\frac{\sigma}{K}\right)^N. \tag{7}$$

3.5. Stress relaxation test analysis

The Norton coefficient (Eq. (7)) can also be measured from stress relaxation tests (Fig. 7), by computing the plastic strain rate as a function of the stress. It is shown in Fig. 8 that the slope becomes lower after irradiation which demonstrates that irradiation induces a decrease of the Norton coefficient. Because of fluctuations of the experimental signal, a direct fitting on the raw signal is also preferred here to the computation of the derivative. Assuming a Norton flow law (Eq. (7)), it can be shown that the stress follows Eq. (8) during the stress relaxation test.

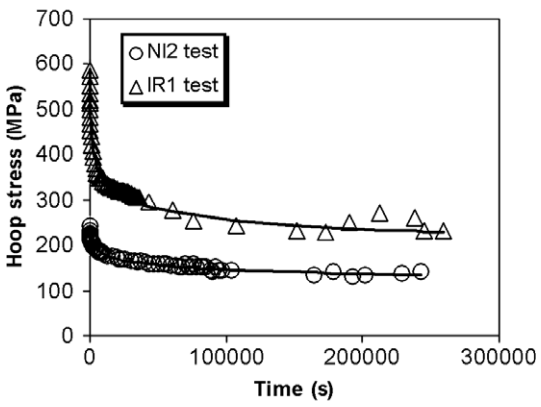

Fig. 7. Stress relaxation tests performed on the specimens NI2 and IR1.

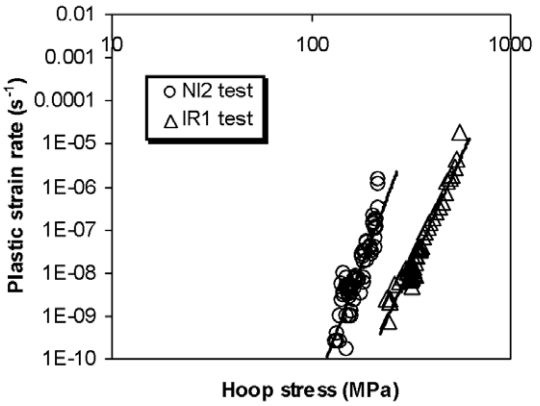

Fig. 8. Plastic strain rate vs. hoop stress for NI2 and IR1 stress relaxation tests.

$$\sigma(t) = \sigma_0(1 + ct)^{\frac{1}{1-N}}. \quad (8)$$

The relaxed stress (σ_{relax}) is given in Table 7 as well as the normalizing coefficient K, the Norton coefficient (N) obtained by the first method, and the three coefficients (σ_0, N, c) obtained by the direct fitting method. The two methods give similar results, nevertheless the direct fitting gives systematically lower values for the Norton coefficient. This analysis proves that irradiation leads to an increase of the strain rate sensitivity (decrease of the Norton coefficient) during stress relaxation tests. It is shown however that for both the non-irradiated material and the irradiated material, the strain rate sensitivity measured during stress relaxation tests is much higher than when measured from the strain hardening tests performed at various strain rates. In other words, the relaxed stress is much higher than the viscous stress. This phenomenon can be explained if a static recovery of the kinematic stress (X) occurs during the stress relaxation test, as described in [20], leading to a high relaxed stress.

Table 7
Relaxed stress and flow law coefficients obtained by stress relaxation test

Test	σ_{relax} (MPa)	First method		Second method		
		K (MPa)	N	σ_0 (MPa)	N (MPa)	c (s^{-1})
NI1	105	820	12.15	230	12	0.0016
NI2	110	780	12.25	245	11.5	0.0022
NI3	115	770	12.48	245	11.8	0.0025
IR1	340	1900	10.14	590	9	0.0074
IR2	300	2110	9.69	560	7.5	0.0007
IR3	290	3020	7.96	500	7.2	0.0007

Table 8
Flow stresses before and after stress relaxation

Test	Hoop stress before relaxation (MPa)	Hoop stress after relaxation (MPa)	Difference of stresses $\Delta\sigma$ (MPa)
NI1	231	248	+16
NI2	243	258	+15
NI3	245	245	0
IR1	587	470	−117
IR2	516	410	−106

3.6. Strain hardening after stress relaxation

Strain hardening tests performed after stress relaxation show that for the non-irradiated material, the flow stress goes rapidly back to the flow stress curve obtained before stress relaxation, whereas for the irradiated material, the flow stress during strain hardening conducted after stress relaxation is much lower (about 100 MPa) than the flow stress curve obtained before stress relaxation as shown in Fig. 1. The flow stresses before and after stress relaxation, when flow stress curve is reached, are given in Table 8. This phenomenon can be attributed to the partial recovery of the isotropic stress during the stress relaxation test performed on the irradiated material. Since this decrease does not reveal itself during the strain hardening but during the stress relaxation, this decrease consists of a static recovery (with time) of the isotropic stress rather than a dynamic recovery (with plastic strain). These phenomena are investigated in more details in the following section using a unified internal variables modeling.

4. Mechanical behavior analysis using an internal variables model

4.1. The model

In order to confirm the previous results and provide a better description of the various mechanical tests, a unified internal variables model [20,33,34] has been used.

Since only one loading direction is studied (internal pressure), the approximation is made that the behavior of the material is isotropic although it is well known that recrystallized zirconium alloy cladding tube behaves anisotropically [23]. However, when the analysis is limited to internal pressure tests ($\sigma_{zz} \approx \sigma_{\theta\theta}/2$ and $\sigma_{rr} \approx 0$), it can be seen that the normal direction of the Mises yield loci is very close to

the normal direction of the Hill yield loci. This shows that this approximation, which seems over-simplified for the general case, leads only to a small error on the plastic flow direction during the simulation when the analysis is limited to internal pressure test. Internal variables modeling which takes into account the anisotropic behavior of Zircaloy tubes as well as the kinematic strain hardening of non-irradiated and irradiated Zircaloy-4 can be found in [23,35]. The behavior of the material is assumed to satisfy the normality law given in Eq. (9).

$$\underline{\underline{\dot{\varepsilon}}}^{p} = \frac{3}{2}\dot{p}\frac{\mathrm{dev}(\underline{\underline{\sigma}}) - \mathrm{dev}(\underline{\underline{X}})}{J_2(\underline{\underline{\sigma}} - \underline{\underline{X}})}, \tag{9}$$

where $\underline{\underline{\dot{\varepsilon}}}^{p}$ is the plastic strain rate tensor and $\dot{p}$ is the equivalent cumulated plastic strain rate defined by Eq. (10). $\mathrm{dev}(\underline{x})$ is the deviator of a second rank tensor (Appendix A) and $J_2(\underline{x})$ is given by Eq. (11). A table of symbols used in the modeling is also given in Appendix A.

$$\dot{p} = \sqrt{\frac{2}{3}\underline{\underline{\dot{\varepsilon}}}^{p} : \underline{\underline{\dot{\varepsilon}}}^{p}}, \tag{10}$$

$$J_2(\underline{x}) = \sqrt{\frac{3}{2}\mathrm{dev}(\underline{x}) : \mathrm{dev}(\underline{x})}. \tag{11}$$

The strain hardening is chosen as additive with two contributions: the kinematic strain hardening and the isotropic strain hardening. These choices are consistent with the Dickson et al. [21] hypothesis concerning the partition of the flow stress stated in Eq. (5). The second rank tensor $\underline{\underline{X}}$, given in Eq. (9), corresponds to the kinematic stress.

The visco-plastic flow law is chosen as a Norton law given in Eq. (12).

$$\dot{p} = \left\langle \frac{J_2(\underline{\underline{\sigma}} - \underline{\underline{X}}) - R}{k} \right\rangle^{n} \tag{12}$$

with $\langle x \rangle = 0$ if $x < 0$ and $\langle x \rangle = x$ if $x \geqslant 0$. The scalar quantity R corresponds to the isotropic stress. The coefficients n and k are the fitting parameters of the flow law.

The kinematic stress is chosen as a classical law [20,33,34] expressed in Eq. (13).

$$\underline{\underline{X}} = \frac{2}{3}C\underline{\underline{\alpha}}, \tag{13}$$

where C is a fitting coefficient and $\underline{\underline{\alpha}}$ is an internal variable second rank tensor. The internal variable $\underline{\underline{\alpha}}$ evolution law is chosen as in Eq. (14) in order to account for the static recovery of the kinematic stress pointed out by the mechanical analysis. D, m and α_0 are three fitting coefficients.

$$\dot{\underline{\underline{\alpha}}} = \underline{\underline{\dot{\varepsilon}}}^{p} - D\underline{\underline{\alpha}}\dot{p} - \left(\frac{J_2(\underline{\underline{\alpha}})}{\alpha_0}\right)^{m}\frac{\underline{\underline{\alpha}}}{J_2(\underline{\underline{\alpha}})}. \tag{14}$$

The unloading tests have shown that the isotropic stress is nearly constant with plastic strain for the non-irradiated material ($\dot{R} = 0$). In the case of the irradiated material, the evolution of the isotropic stress with plastic strain has not been measured. Only a minimum value at 0.2% plastic strain for the isotropic stress has been obtained. Nevertheless, since sweeping up of loops occurs inside channels, the isotropic strain hardening is believed to be very low. The isotropic strain hardening is therefore chosen as constant with plastic strain as for the non-irradiated material. The static recovery of the isotropic stress, revealed by the strain hardening test performed after stress relaxation, is taken into account in Eq. (15).

$$\dot{R} = -b(R - R_0) \tag{15}$$

with $R(0) = R_0 + \Delta R$. $\dot{R}$ is the time derivative of the isotropic stress and b, R_0 and ΔR are three fitting coefficients. For the non-irradiated material the coefficients are $b = 0$ and $\Delta R = 0$.

Only the internal pressure tests NI1, NI4, NI7, IR1 and IR2 performed on non-irradiated and irradiated M5™ claddings are used for the fitting. The model has 11 coefficients: two coefficients for elasticity, Young's modulus Y and Poisson's ratio v, two for the flow law (n, k), four coefficients for the kinematic hardening (C, D, m, α_0) and three for the isotropic stress $(R_0, b, \Delta R)$. Since only the hoop strain is measured during internal pressure test, the Poisson's ratio is not fitted and chosen as $v = 0.42$, value close to the ones given in [23,36]. The fitting procedure consists of introducing the experimentally measured parameters given in Tables 4–7 as initial parameters. Then coefficients are adjusted separately for non-irradiated and irradiated materials using a minimizing procedure of a cost function.

The viscous stress, the isotropic stress and the kinematic stress are also computed during the simulation and compared to experimental values. The computed viscous stress is defined [20,33], according to the chosen model, and in agreement with the Dickson et al. [21] hypothesis (Eq. (5)), as Eq. (16).

$$\sigma_V = \langle J_2(\underline{\underline{\sigma}} - \underline{\underline{X}}) - R \rangle = k(\dot{p})^{\frac{1}{n}}. \tag{16}$$

Since the kinematic stress is a second rank tensor, the computed value for the kinematic stress is

chosen as the hoop component $X_{\theta\theta}$. However, since the internal pressure test is a biaxial loading and because of the chosen flow law, the computed value of the hoop stress of the kinematic stress ($X_{\theta\theta}$) cannot be directly compared to the value of the kinematic stress (X) measured in the hoop direction reported in the mechanical analysis part. Only orders of magnitude and relative proportion for R_0, σ_V and $X_{\theta\theta}$ are compared to measured values.

4.2. Results

The two coefficients sets (NI and IR coefficients sets) obtained after the fitting procedure are given in Table 9. A good agreement is obtained between simulated tests and experimental tests as shown in Figs. 9 and 10 (NI1 and IR1 tests). It can be noticed that a decrease of the Young modulus with irradiation is obtained (≈10%), probably mainly because of the two different mechanical test devices used for non-irradiated and irradiated materials. This phenomenon could also be explained with analogy to the microplasticity phenomenon (reversible motion of dislocations) which induces a decrease of the apparent Young modulus with plastic strain for non-irradiated strain hardened materials [37,38]. The fitting sensitivity has been analyzed using numerical perturbations. Coefficients values have been modified from 1% to 10%. The relative change in the cost function has been computed. A perturbation lower than 10%, for low sensitivity coefficients, leads to a small change in the cost function. While a change higher than 1%, for highly sensitive coefficients, leads to a significant change in the cost function. Estimated uncertainties on coefficients are given in Table 9. A high sensitivity is obtained for the Young modulus (Y), for exponent values n and m, for the C coefficient and for the yield stress coefficients R_0 and ΔR.

Table 9
Coefficients of the model obtained after the fitting procedure

Coefficient	Non-irradiated	Irradiated	Uncertainty (%)
Y (MPa)	89 500	79 700	±1
ν^*	0.42	0.42	–
n	13.0	6.2	±1
k (MPa s$^{1/n}$)	130	520	±10
R_0 (MPa)	100	140	±1
b (s^{-1})	0	4×10^{-6}	±10
ΔR (MPa)	0	60	±1
C (MPa)	8700	501 000	±1
D	80	3000	±10
m	1.7	1.5	±1
α_0 (s$^{1/M}$)	24	16	±10

*Fixed coefficient.

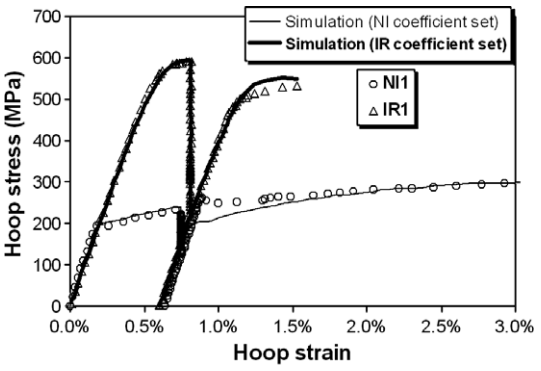

Fig. 9. Stress–strain curve of the tests NI1 and IR1 and simulated tests using the NI coefficients set and the IR coefficients set.

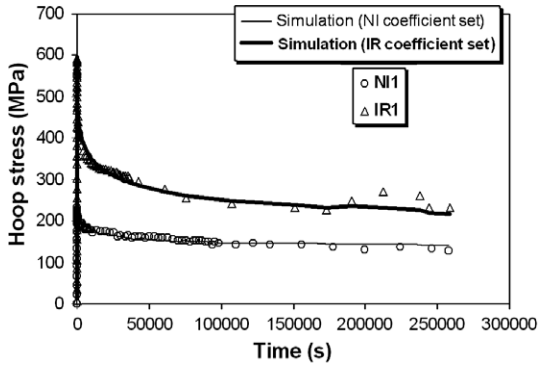

Fig. 10. Stress–time curve of the tests NI1 and IR1 and simulated test using the NI coefficients set and the IR coefficients set.

The use of this simple model allows to confirm that the strain rate sensitivity increases with irradiation as shown by the decrease of the n coefficient with irradiation ($n = 13.0$ for the non-irradiated material and $n = 6.2$ for the irradiated material). It has also been confirmed that in order to reproduce the low strain rate sensitivity in strain hardening as well as the stress relaxation, static recovery of the kinematic hardening has to be introduced into the modeling. This simple internal variables modeling has also confirmed that the strain hardening rate at the onset of plastic flow is increased by irradiation as shown by the increase of the C coefficient ($C = 8.7$ GPa for non-irradiated material and $C = 501$ GPa for irradiated material). It has also been confirmed that the strain hardening rate decreases more rapidly than for the irradiated material as proved by the increase with irradiation of the

D coefficient ($D = 80$ for the non-irradiated material and $D = 3000$ for the irradiated material). The introduction of the static recovery of the isotropic stress has also been able to reproduce the decrease of the flow stress, for strain hardening test performed after stress relaxation in the case of the irradiated material.

Finally, a major interest of this approach is the ability to compute and estimate the kinematic, isotropic and viscous stresses (Figs. 11–14) and compare them to measured values or bounds obtained by the Handfield and Dickson technique. It is proposed here that for the irradiated material, the isotropic stress (R) is equal to 200 MPa and that the kinematic stress (here $X_{\theta\theta}$) is equal to 200 MPa at 0.2% plastic strain. This has to be compared to the values estimated for the non-irradiated material where the isotropic stress (R) is equal to 100 MPa and the kinematic stress (here $X_{\theta\theta}$) is equal to 100 MPa at 1.5% plastic strain. The simple internal variables model used shows that these values are consistent with the mechanical behavior of the material.

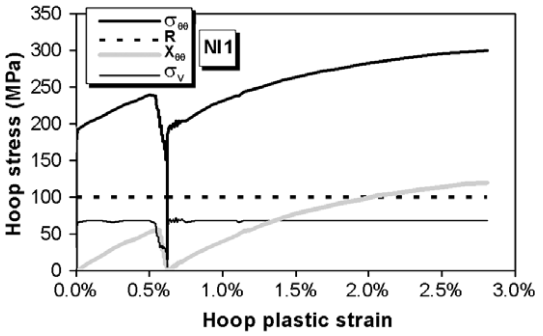

Fig. 11. Simulated values for isotropic, viscous and kinematic stresses for the test NI1 vs. hoop plastic strain.

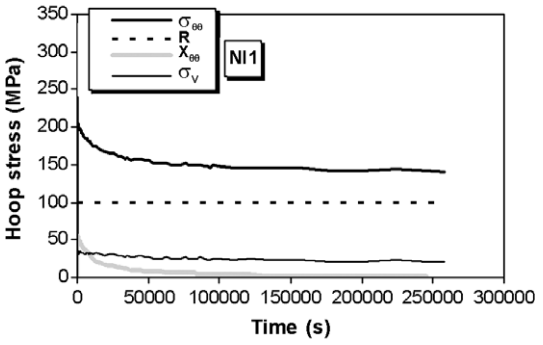

Fig. 12. Simulated values for isotropic, viscous and kinematic stresses for the test NI1 vs. time.

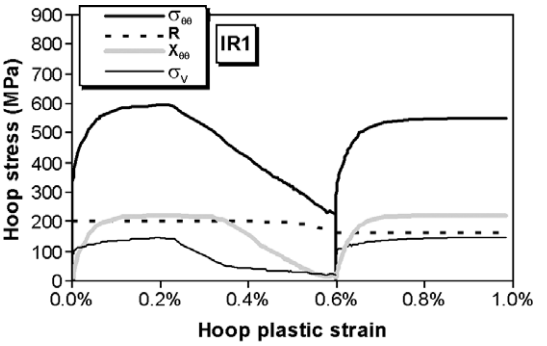

Fig. 13. Simulated values for isotropic, viscous and kinematic stresses for the test IR1 vs. hoop plastic strain.

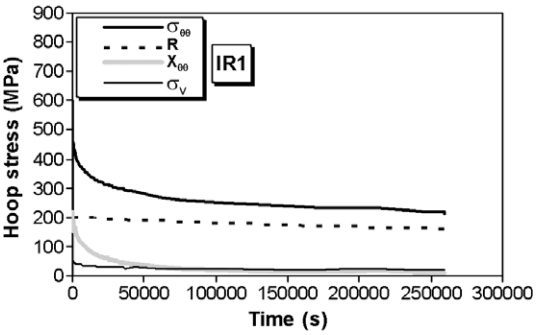

Fig. 14. Simulated values for isotropic, viscous and kinematic stresses for the test IR1 vs. time.

5. Discussions

5.1. Discussion on the mechanical behavior of the non-irradiated material

Mechanical properties obtained in this study for the non-irradiated material agree with mechanical properties reported in the literature for recrystallized zirconium alloys at 350 °C [23–31]. The Handfield and Dickson technique [21], applied to non-irradiated recrystallized zirconium alloys, has shown that the isotropic stress (R) is constant during strain hardening. According to [22], this phenomenon can be attributed to the low hardening due to athermal short range obstacles such as forest dislocations. Indeed it has been recently demonstrated in [39] that, in α-Zr, the forest hardening of ⟨a⟩ screw dislocations gliding in the prismatic plane (principal slip system as reviewed by [40,41]) is very low at room temperature. The analysis proposed by Handfield and Dickson has also shown that the viscous stress is low (σ_V is of the order of

20 MPa) and constant with plastic strain for non-irradiated Zr alloys at 350 °C. This result is confirmed by the very low strain rate sensitivity observed during strain hardening at various strain rates, which proves that the viscous stress is close to zero. The low strain rate sensitivity of the non-irradiated material has been reported by many authors [24–31]. This phenomenon is usually attributed to dynamic strain aging effect due to the interaction of oxygen solute atoms with ⟨a⟩ screw dislocations gliding in the prismatic plane. These tests have also shown that the strain hardening is mainly due to the increase of kinematic stress since only the kinematic stress (X) increases with plastic strain. According to [22,24,25,42–45], this phenomenon is attributed to strain incompatibilities between grains due to the plastic anisotropy of the h.c.p. grains which present a limited number of easy glide slip systems. It has also been shown that a part of the kinematic stress (X) is recovered during the stress relaxation test. This explains the higher strain rate sensitivity measured during stress relaxation test than during strain hardening test.

5.2. Discussion on the mechanical behavior of the irradiated material

It has been shown that irradiation leads to a strong hardening, as reported in Fig. 1 and Table 3 for yield stress ($\sigma_{0.02\%}$) and flow stress at 0.2% ($\sigma_{0.2\%}$). The increase of the yield stress ($\sigma_{0.02\%}$) with irradiation can directly be related to the high loop density induced by irradiation. Indeed, according to the classical dispersed barrier hardening model reviewed by [6,7], dislocation loops act as obstacles against dislocation glide. However, if a sufficient shear stress is applied, dislocations overcome or sweep up all obstacles encountered in the slip planes, thus macroscopic plastic strain occurs [8]. This stress level defines the macroscopic yield stress chosen here as the flow stress at very low plastic strain (0.02% plastic strain).

The mechanical analysis also shows that the flow stress at 0.2% plastic strain is increased by irradiation. In this case however, TEM investigations of the specimen IR5 [16] have proved that for 0.2% plastic strain, basal channels are observed. It is surprising that irradiation hardening is still observed for this plastic strain level although irradiation loops are cleared up inside channels. Additionally, it is seen in Fig. 1 that for the specimen IR4 the flow stress increases from 0.2% to 0.5% plastic strain and that many channels can be observed at 0.5% plastic strain, as reported in [16]. It can be assumed that for the specimen IR4 channels are already present in the material for 0.2% plastic strain as it has been observed in the specimen IR5. Thus, it is also surprising that the flow stress increases, since dislocation channeling corresponds to irradiation defects clearing, and therefore to local softening inside channels. This phenomenon can be explained by considering the polycrystalline aspect of the material. Indeed, the localization of the plastic strain inside a channel should lead to high strain incompatibility between the channel and the surrounding grains which should induce back stress due to dislocations pile-up at grain boundaries. Indeed, it has been proved for various materials [22] that intragranular heterogeneous plastic deformation can induce internal stress or back stress. For instance, in the case of the low cycle fatigue, various authors have suggested that heterogeneous plastic deformation such as planar slip or persistent slip band induce internal stress or back stress [22,46,47]. Additionally, since basal channeling occurs exclusively for internal pressure tests, only two independent deformation modes are activated and compatibility conditions between grains cannot be satisfied [41]. This phenomenon should also induce microscopic internal stresses and eventually should lead to the activation of other deformation modes. These microscopic internal stresses are associated, at the macroscopic scale, to the kinematic hardening component of the flow stress. Therefore, in the case of the irradiated material a strong kinematic hardening is expected to occur. This high kinematic hardening can then balance the local softening inside channels (decrease of the isotropic stress), leading to a hardening behavior at the macroscopic scale as observed for the specimen IR4. This would therefore explain that the plastic deformation at the specimen scale is still homogeneous, according to laser measurements given in [16], although at the grain scale, the plastic deformation is localized inside channels.

The high strain hardening rate measured at the onset of plastic flow in the case of the irradiated material can also be interpreted as a consequence of the localization of the plastic strain at the grain scale. Indeed, if a channel embedded into an elastic medium is considered, a high amount of plastic strain inside the channel is required in order to generate a small amount of macroscopic plastic strain. This high amount of local plastic strain will then

lead to a high increase of internal stress and thus to a high macroscopic strain hardening rate. It is shown however that the strain hardening rate decreases very rapidly in the case of the irradiated material (Fig. 2) compared to the non-irradiated material. The decrease of the strain hardening rate can mainly be attributed to the propagation of channels from grain to grain due to the high stress concentration at grain boundaries, at the edge of channels, as it has been observed in [16,17]. The decrease of the macroscopic strain hardening rate would eventually induce strain localization at the specimen scale. This can explain the strong decrease in uniform elongation with irradiation reported by many authors [1–4,10,11,14,48,49]. Nevertheless, using internal pressure tests, it has not been possible to measure the kinematic stress, only a maximum value has been obtained ($X \leqslant 235$ MPa). Kinematic strain hardening in compression–tension tests for the transverse direction has not yet been experimentally observed for irradiated zirconium alloys due to the difficulty to perform appropriate mechanical test. Nevertheless, the stabilized hysteresis loop, obtained during fatigue testing experiment [50] performed in the axial direction on irradiated Zy-4 and Zy-2 proves that a stronger Bauschinger effect occurs after irradiation. This observation supports the hypothesis that kinematic strain hardening is also strong for internal pressure tests.

It has also been shown that irradiation leads to an increase of the strain rate sensitivity. This phenomenon is attributed to the basal slip activation instead of the prismatic slip activation. Indeed, the secondary slip systems are expected not to undergo dynamic strain aging for this test temperature, leading to higher strain rate sensitivity [51]. This phenomenon has also been reported by Pettersson et al. [32] for internal pressure test performed at 290 °C, however Yasuda et al. [3] has not observed any increase of strain rate sensitivity on Zy-2 tested in axial direction. This can be explained by the fact that in this case prismatic channeling occurs instead of basal channeling [16]. The plastic strain localization inside channels can also induce an increase of the strain rate sensitivity since the local strain rate inside channels is higher than the macroscopic strain rate leading therefore to a higher viscous stress. As for the non-irradiated material, it has also been shown that a static recovery of the kinematic stress (X) occurs during stress relaxation tests leading to a higher strain rate sensitivity during strain relaxation test than during strain hardening test.

Strain hardening test performed after stress relaxation test have suggested that a static recovery of the isotropic stress also occurs during stress relaxation test. The recovery of the isotropic stress can be explained by the sweeping up of ⟨a⟩ loops by gliding dislocations inside channels. However, this decrease should correspond to a dynamic recovery of ⟨a⟩ loops with plastic strain which is not in agreement with the macroscopic analysis. Although dynamic recovery of ⟨a⟩ loops occurs at the microscopic scale it is possible that this dynamic recovery does not appear at the macroscopic scale due to the polycrystalline aspect of the material. Indeed, as it has been discussed previously, the polycrystalline aspect of the material can induce internal stresses (or kinematic stress) which can balance the local softening inside channels. However, once the material is reloaded, the flow stress is likely to be lower than that observed prior stress relaxation, as observed experimentally. It is also possible that thermal annealing of ⟨a⟩ loops occurs for stress relaxation tests performed during 72 h at 350 °C. This thermal annealing should lead to a static recovery of the isotropic stress, as observed at the macroscopic scale. Nevertheless, the static recovery of ⟨a⟩ loops was not obvious from the TEM investigations performed in [17].

6. Conclusions

A specific mechanical behavior analysis has been performed for non-irradiated and irradiated recrystallized zirconium alloys. By means of this specific analysis, confirmed by an internal variables modeling, it has been shown that neutron radiation induces major changes in the mechanical behavior of recrystallized zirconium alloys. Indeed it has been assessed that irradiation leads to a strong increase of the yield stress as well as the isotropic stress. This has been attributed to the hardening due to the high loop density induced by irradiation. It has also been proved that the strain rate sensitivity, as well as the associated viscous stress, is increased by irradiation which is explained by the activation of basal slip instead of prismatic slip for the non-irradiated material. From TEM examinations and mechanical analysis it has been proposed that the kinematic strain hardening is increased by irradiation due to the high strain incompatibilities between grains induced by the activation of basal channeling. The increase of kinematic strain hardening with irradiation can explain the increase with irradiation of the

strain hardening rate at the onset of plastic flow. It is also proposed that the fast decrease of the strain hardening rate of the irradiated material is attributed to the propagation of basal channels from grain to grain. Nevertheless, the kinematic stress has not been measured for the irradiated material. The mechanical analysis has also proved that the strain rate sensitivity in stress relaxation, as well as the associated relaxed stress, is increased by irradiation. This is attributed to the activation of the basal slip as well as the important recovery of the kinematic stress during relaxation test due to the increase of the kinematic stress with irradiation.

Acknowledgements

The authors thank EdF and AREVA-NP for supporting this study.

Appendix A. Table of symbols used in the modeling

The deviator of a second rank tensor is defined as $\mathrm{dev}(\underline{x}) = \underline{x} - \frac{1}{3}\mathrm{tr}(\underline{x})\underline{I}$ where $\mathrm{tr}(\underline{x})$ is the trace of a two orders tensor. The constricted product $\underline{x}:\underline{y}$ is defined, using Einstein's notation, by $\underline{\underline{x}}:\underline{\underline{y}} = x_{ij}y_{ij}$.

Symbol	Variables and coefficients
$\underline{\underline{\sigma}}$	Stress
$\underline{\underline{\varepsilon}}$	Strain
$\underline{\underline{\dot{\varepsilon}}}^{\mathrm{p}}$	Plastic strain rate
$\dot{p}$	Cumulated equivalent plastic strain rate
$\underline{\underline{\alpha}}$	Internal variable for the kinematic hardening
$\underline{\underline{X}}$	Kinematic stress
σ_{V}	Viscous stress
R	Isotropic stress
$\dot{R}$	Time derivative of the isotropic stress
Y	Young modulus
v	Poisson's ratio
n	Flow law exponent
k	Fitting coefficient of the flow law
R_0	Fitting coefficients for the static recovery
b	of the isotropic stress
ΔR	
C	Fitting coefficients for the kinematic
D	strain hardening evolution law
m	
α_0	

References

[1] H.R. Higgy, F.H. Hammad, J. Nucl. Mater. 44 (1972) 215.
[2] C.J. Baroch, in: Properties of Reactor Structural Alloys after Neutron or Particle Irradiation, ASTM STP 570, 1975, p. 129.
[3] T. Yasuda, M. Nakatsuka, K. Yamashita, in: Zirconium in the Nuclear Industry: 7th International Symposium, ASTM STP 939, 1987, p. 734.
[4] G.F. Rieger, D. Lee, in: Zirconium in Nuclear Applications, ASTM STP 551, American Society for Testing Materials, 1974, p. 355.
[5] D.O. Northwood, R.W. Gilbert, L.E. Bahen, P.M. Kelly, R.G. Blake, A. Jostsons, P.K. Madden, D. Faulkner, W. Bell, R.B. Adamson, J. Nucl. Mater. 79 (1979) 379.
[6] A.L. Bement, in: Second International Conference on the Strength of Metals and Alloys ASM Metals Pk., vol. 2, 1970, p. 693.
[7] P.B. Hirsch, in: Proceedings of a Conference on Point Defect Behavior and Diffusional Processes, University of Bristol, 13–16 September 1976.
[8] M.S. Wechsler, Dislocation Channeling in Irradiated and Quenched Metals. The Inhomogeneity of Plastic Deformation, ASM, Metals Park, OH, 1973, p. 19.
[9] C.E. Coleman, D. Mills, J. van der Kuur, Can. Metall. Quater. 11 (1972) 91.
[10] T. Onchi, H. Kayano, Y. Higashiguchi, J. Nucl. Mater. 88 (1980) 226.
[11] C.D. Williams, R.B. Adamson, K.D. Olhausen, in: European Conference on Irradiation Behavior of Fuel Cladding and Core Component Materials, Karlsruhe, 1974, p. 189.
[12] K. Pettersson, J. Nucl. Mater. 105 (1982) 341.
[13] R.B. Adamson, W.L. Bell, in: International Symposiums, vol. 1, Xian, China, 1985, p. 237.
[14] M. Fregonese, C. Régnard, L. Rouillon, T. Magnin, F. Lefebvre, C. Lemaignan, in: Zirconium in Nuclear Industry: 12th International Symposium, ASTM STP 1354, 2000, p. 377.
[15] C. Régnard, B. Verhaeghe, F. Lefebvre-Joud, C. Lemaignan, in: Zirconium in the Nuclear Industry, 13th International Symposium, ASTM STP 1423, 2002, p. 384.
[16] F. Onimus, I. Monnet, J.L. Béchade, C. Prioul, P. Pilvin, J. Nucl. Mater. 328 (2004) 165.
[17] F. Onimus, J.L. Béchade, C. Prioul, P. Pilvin, I. Monnet, S. Doriot, B. Verhaeghe, D. Gilbon, L. Robert, L. Legras, J.-P. Mardon, J. ASTM Int., vol. 2, no. 8, 2005, and Zirconium in the Nuclear Industry: 14th International Symposium, ASTM STP 1467, 2006, p. 53.
[18] A.H. Cottrell, Dislocations and Plastic Flow in Crystals, Oxford University, London, 1953, p. 111.
[19] D. Kuhlmann-Wilsdorf, C. Laird, Mater. Sci. Eng. 37 (1) (1979) 111.
[20] J. Lemaitre, J.L. Chaboche, Mechanics of Solid Materials, Cambridge University, 1990.
[21] J.I. Dickson, J. Boutin, L. Handfield, Mater. Sci. Eng. 64 (1984) L7.
[22] X. Feaugas, Recent Re. Devel. Mater. Sci. 4 (2003) 35.
[23] P. Delobelle, P. Robinet, P. Geyer, P. Bouffioux, J. Nucl. Mater. 238 (1996) 135.
[24] J. Crépin, T. Bretheau, D. Caldemaison, F. Ferrer, Acta Mater. 48 (2000) 505.

[25] C. Li, S. Ying, B. Shen, S. Qui, X. Ling, Y. Wang, Q. Peng, J. Nucl. Mater. 321 (2003) 60.
[26] K.W. Lee, S.K. Kim, K.T. Kim, S.I. Hong, J. Nucl. Mater. 295 (2001) 21.
[27] J.L. Derep, S. Ibrahim, R. Rouby, G. Fantozzi, Acta Metall. 28 (1980) 607.
[28] S.I. Hong, H.J. Kim, Mater. Sci. Eng. 86 (1987) L1.
[29] T.K. Sinha, M.K. Asundi, J. Nucl. Mater. 67 (1977) 311.
[30] D. Mills, G.B. Craig, Trans. Metall. Soc. AIME 242 (1968) 1881.
[31] F. Ferrer, A. Barbu, T. Bretheau, J. Crépin, F. Willaime, D. Charquet, in: Zirconium in Nuclear Industry, 13th Symposium, ASTM STP 1423, 2002, p. 863.
[32] K. Petterson, G. Versterlund, T. Andersson, in: Zirconium in the Nuclear Industry (Fourth Conference), ASTM STP 681, 1979, p. 155.
[33] J.L. Chaboche, G. Rousselier, J. Pressure Vessel Technol. 105 (1983) 153.
[34] J.L. Chaboche, Int. J. Plast. 5 (1989) 247.
[35] I. Schaffler, P. Geyer, P. Bouffioux, P. Delobelle, Trans. ASME 122 (2000) 168.
[36] E.B. Schwenk, K.R. Wheeler, G.D. Shearer, J. Nucl. Mater. 73 (1978) 129.
[37] H.M. Ledbetter, M.W. Austin, Phys. State Sol. (a) 104 (1987) 203.
[38] S. Frénois, E. Munier, X. Feaugas, P. Pilvin, J. Phys. IV France 11 (2001) 301.
[39] G. Monnet, B. Devincre, L.P. Kubin, Acta Mater. 52 (2004) 4317.
[40] D.L. Douglass, The Metallurgy of Zirconium, Atomic Energy Review Supplement, International Atomic Energy Agency, Vienna, 1971, p. 41.
[41] E. Tenckhoff, in: Deformation Mechanisms, Texture and Anisotropy in Zirconium and Zircaloy, ASTM STP 966, 1988, p. 1.
[42] s.R. MacEwen, C.E. Ells, O.T. Woo, J. Nucl. Mater. 101 (1981) 336.
[43] J.W.L. Pang, T.M. Holden, P.A. Turner, T.E. Mason, Acta Mater. 47 (2) (1999) 373.
[44] P.A. Turner, N. Christodoulou, C.N. Tomé, Int. J. Plast. 11 (3) (1995) 251.
[45] N. Christodoulou, Acta Metall. 37 (2) (1989) 529.
[46] O.B. Pedersen, in: J. Lepinoux et al. (Eds.), Multiscale Phenomena in Plasticity, Kluwer Academic Publishers, 2000, p. 83.
[47] H. Mughrabi, Mater. Sci. Eng. A317 (2001) 171.
[48] D. Lee, R.B. Adamson, in: Zirconium in the Nuclear Industry, ASTM STP 633, 1977, p. 385.
[49] H.S. Rosenbaum, G.F. Rieger, D. Lee, Metall. Trans. 5 (1974) 1867.
[50] S.B. Wisner, M.B. Reynolds, R.B. Adamson, in: Zirconium in the Nuclear Industry: 10th International Symposium, ASTM STP 1245, 1994, p. 599.
[51] H. Conrad, Prog. Mater. Sci. 26 (1981) 123.